

Induced diffusion of internal gravity waves: directionality and role in ocean mixing

Yue Cynthia Wu o and Yulin Pan o

¹Naval Architecture and Marine Engineering, University of Michigan, Ann Arbor, MI, USA **Corresponding author:** Yue Cynthia Wu, ywu.ocean@gmail.com

(Received 1 May 2025; revised 18 August 2025; accepted 24 September 2025)

Induced diffusion (ID), an important mechanism of spectral energy transfer due to interacting internal gravity waves (IGWs), plays a significant role in driving turbulent dissipation in the ocean interior. In this study, we revisit the ID mechanism to elucidate its directionality and role in ocean mixing under varying IGW spectral forms, with particular attention to deviations from the standard Garrett-Munk spectrum. The original interpretation of ID as an action diffusion process, as proposed by McComas et al., suggests that ID is inherently bidirectional, with its direction governed by the vertical-wavenumber spectral slope σ of the IGW action spectrum, $n \propto m^{\sigma}$. However, through the direct evaluation of the wave kinetic equation, we reveal a more complete depiction of ID, comprising both a diffusive and a scale-separated transfer rooted in the energy conservation within wave triads. Although the action diffusion may reverse direction depending on the sign of σ (i.e. red or blue spectra), the net transfer by ID consistently leads to a forward energy cascade at the dissipation scale, contributing positively to turbulent dissipation. This supports the viewpoint of ID as a dissipative mechanism in physical oceanography. This study presents a physically grounded overview of ID, and offers insights into the specific types of wave-wave interactions responsible for turbulent dissipation.

Key words: internal waves, waves in rotating fluids, ocean processes

1. Introduction

Internal gravity waves (IGWs) are ubiquitous features of the ocean and are generated when stratified fluids are perturbed. The oceanic IGW field is primarily energised at large scales by atmospheric and tidal forcings, and dissipated at small scales. Given the scale separation between forcing and dissipation, interscale energy transfer is crucial for sustaining an energy cascade across the IGW continuum. Mechanisms facilitating this interscale energy transfer include wave—wave interactions (e.g. Hasselmann 1966;

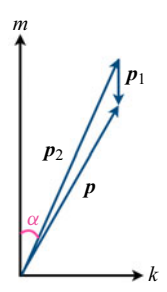


Figure 1. A resonant wave triad $p = p_1 + p_2$ typical of the induced diffusion (ID) mechanism. The angle α between the wavenumber vector and the vertical is positively correlated with the wave frequency according to the dispersion relation.

Hasselmann, Saffman & Lighthill 1967), wave-mean/eddy interactions (e.g. Kafiabad, Savva & Vanneste 2019; Dong *et al.* 2020, 2023; Savva, Kafiabad & Vanneste 2021; Delpech *et al.* 2024), and bottom scattering (e.g. Kunze & Llewellyn Smith 2004). Of these pathways, wave—wave interactions are regarded in many studies as the dominant process in the interior of the ocean (Polzin & Lvov 2011; Polzin *et al.* 2014).

The study of interscale energy transfer via wave—wave interactions was pioneered by McComas *et al.* in a series of publications (McComas & Bretherton 1977*a*; McComas 1977; McComas & Müller 1981*a,b*). These works posited that interscale energy transfer is dominated by three types of non-local interactions (i.e. wave triads that are scale-separated in vertical wavenumber, frequency, or both), namely parametric subharmonic instability, elastic scattering, and ID. This framework laid the theoretical foundation for finescale parameterization to infer turbulent dissipation (Henyey, Wright & Flatté 1986; Gregg 1989; Polzin *et al.* 1995, 2014), but it has recently been shown to be incorrect due to the overlooked role of local interactions (Dematteis, Polzin & Lvov 2022; Wu & Pan 2023).

The present work focuses on the ID mechanism, one of the three types of non-local interactions. ID describes the scattering of a high-frequency, high-vertical-wavenumber wave by a low-frequency, low-vertical-wavenumber wave, resulting in the generation of another high-frequency, high-vertical-wavenumber wave through resonant interactions. The dynamics at small scales (represented by p and p_2 in figure 1) has been shown to satisfy a diffusion equation in terms of wave action n (defined as wave energy E divided by intrinsic frequency ω), driving a diffusive cascade across vertical wavenumber m (McComas & Bretherton 1977b):

$$\frac{\partial n(\mathbf{p})}{\partial t} = \frac{\partial}{\partial m} \left[D_{33} \frac{\partial}{\partial m} n(\mathbf{p}) \right]. \tag{1.1}$$

Here, $p = (k_x, k_y, m)$ denotes the three-dimensional wavenumber vector. Vertical diffusivity D_{33} , being the dominant component of the three-dimensional diffusion tensor, is determined by the shear content of the large-scale wave p_1 (figure 1). (An alternative perspective presented by Lanchon & Cortet (2023) demonstrates that ID conserves the ratios $\omega/|m|$ and k/m^2 within a wave triad.) Assuming a stationary large-scale field where $n(p_1)$ and D_{33} remain constant, McComas & Müller (1981a) evaluated the downscale energy flux towards higher m using (1.1), assuming a logarithmic correction $n \propto -\ln(m)$ at small scales to the standard Garrett–Munk (GM) spectrum. Turbulent dissipation is then approximated by the flux across the dissipation scale, where IGWs become unstable to shear instability, and break at vertical scales smaller than 10 m. As a result, ID was estimated

to account for approximately 20 % of the total turbulent dissipation (McComas & Müller 1981a), with the remainder attributed to parametric subharmonic instability.

McComas's viewpoint on ID is not without problems under closer scrutiny. For the GM spectrum characterised by $n \propto m^0$ at small scales (Cairns & Williams 1976), ID vanishes since the action spectrum displays no gradient in m. While secondary diffusion can arise from off-diagonal components in the diffusion tensor (Dematteis et al. 2022), the relative contribution of ID to the total turbulent dissipation is certainly much less than that postulated by McComas et al. The situations for spectra deviating from GM are even more elusive, despite being commonly observed in field measurements (Polzin & Lyov 2011). Since diffusion always acts in the down-gradient direction, ID has the potential to reverse direction depending on the relative action intensity between the two small-scale waves, p and p_2 , in a single triad (figure 1). For an IGW spectrum, this direction is consequently governed by the sign of the vertical-wavenumber spectral slope σ of the action spectrum at small scales, $n \propto m^{\sigma}$. Specifically, for a blue or red action spectrum with positive or negative σ , the action diffusion at small scales corresponds to a backward or forward cascade, respectively. Does this imply that ID can contribute negatively to turbulent dissipation? This is a perplexing question, particularly given the long-standing consensus within the community that ID is a dissipative mechanism, as neither observational nor numerical evidence has reported a scenario involving a backward ID transfer (e.g. Pan et al. 2020; Skitka et al. 2024).

Via direct evaluation of the wave kinetic equation (WKE), we now have a clear answer to the above question: for GM-like spectra adhering to specific spectral forms as detailed in Appendix A, ID always contributes positively to turbulent dissipation. This finding arises from the inclusion of a previously unrecognised scale-separated transfer occurring between the large-scale wave p_1 and the two small-scale waves, p and p_2 (figure 1). This is in addition to the well-established diffusive transfer between the two small-scale waves, p and p_2 , as described by (1.1). Physically, the scale-separated transfer is a direct consequence of energy conservation, since the diffusive transfer conserves action but not energy. Although McComas & Müller (1981b) recognised the indispensable role of scale-separated transfer in conserving energy within wave triads, computational limitations in the 1980s necessitated treating the large-scale wave as an 'external field' that did not actively participate in energy/action exchanges with the two small-scale waves. This simplification allowed for the theoretical reduction of ID to a diffusion problem (1.1), but it confined attention to the diffusive transfer at small scales for decades thereafter.

Leveraging advancements in high-performance computing, we can now evaluate the full WKE without adopting heuristic assumptions, thereby enabling exploration of the complete dynamics of the ID mechanism. The energy flux across a specified vertical scale emerges as a combined result of both scale-separated and diffusive transfers: for an action spectrum that is red or blue in m, the diffusive or scale-separated transfer dominates near the 10 m vertical scale, respectively, leading to a consistently positive effect on ocean mixing. We conclude by quantifying the relative contribution of ID to the total turbulent dissipation, and examining the connection between the WKE results and finescale parameterization.

2. Methodology

2.1. The Wave kinetic equation (WKE)

The WKE describes the evolution of the wave action spectrum under interactions of weakly nonlinear waves, providing a framework for understanding the energy transfer

across scales. For IGWs, the WKE is given by

$$\frac{\partial n(\boldsymbol{p},t)}{\partial t} = \iint 4\pi |V(\boldsymbol{p}, \boldsymbol{p}_1, \boldsymbol{p}_2)|^2 \mathcal{F}_{p12} \delta(\omega - \omega_1 - \omega_2) \delta(\boldsymbol{p} - \boldsymbol{p}_1 - \boldsymbol{p}_2) d\boldsymbol{p}_1 d\boldsymbol{p}_2
- \iint 8\pi |V(\boldsymbol{p}_1, \boldsymbol{p}, \boldsymbol{p}_2)|^2 \mathcal{F}_{1p2} \delta(\omega_1 - \omega - \omega_2) \delta(\boldsymbol{p}_1 - \boldsymbol{p} - \boldsymbol{p}_2) d\boldsymbol{p}_1 d\boldsymbol{p}_2.$$
(2.1)

The right-hand side of (2.1), namely the collision integral, describes the time evolution of the wave action density at a given wavenumber p due to triad interactions with two other components, p_1 and p_2 , satisfying the resonant conditions $p = p_1 \pm p_2$ and $\omega = \omega_1 \pm \omega_2$. The functions $\mathcal{F}_{p12} = n_1 n_2 - n_p (n_1 + n_2)$ and $\mathcal{F}_{1p2} = n_p n_2 - n_1 (n_p + n_2)$ are quadratic in terms of wave action, where n_p is shorthand for n(p, t), n_1 for $n(p_1, t)$, and so on. The interaction kernel V has been derived using various methods for hydrostatic (e.g. McComas 1977; Lvov & Tabak 2001, 2004; Lvov et al. 2010) and non-hydrostatic (e.g. Olbers 1974, 1976; Müller & Olbers 1975; Labarre et al. 2024e) set-ups. Notably, the interaction kernel from derivations up to Lvov et al. (2010) has been demonstrated to be equivalent on the resonant manifold (Lvov, Polzin & Yokoyama 2012).

An important metric to characterise the nonlinearity level of wave–wave interactions is the normalised Boltzmann rate (Nazarenko 2011; Lvov *et al.* 2012), which is the ratio between the linear time scale (wave period) τ^L and the nonlinear time scale τ^{NL}

$$Bo \equiv \frac{\tau^L}{\tau^{NL}} = \frac{2\pi}{\omega} \frac{\partial E/\partial t}{E}.$$
 (2.2)

The normalised Boltzmann rate establishes a criterion for interpreting the WKE results within specific spectral regimes. Theoretically, the WKE (2.1) is valid only when $|Bo| \ll 1$, as implied by the weakly nonlinear assumption underlying wave turbulence theory (Zakharov, Lvov & Falkovich 1992; Nazarenko 2011).

Although earlier results based on the work of McComas *et al.* often relied on heuristic assumptions, such as the (overly) simplified collision integral, recent advances in high-performance computing have allowed for direct evaluation of the complete collision integral for general spectral forms (Eden *et al.* 2019*a,b*, 2020; Dematteis & Lvov 2021; Dematteis *et al.* 2022, 2024; Lanchon & Cortet 2023; Wu & Pan 2023; Labarre *et al.* 2024*a,b*). The WKE has since been applied to global datasets of IGW spectra and benchmarked by finescale parameterization and microstructure observations (Dematteis *et al.* 2024), establishing itself as a powerful tool for estimating turbulent dissipation and improving parameterizations of ocean mixing in general circulation and climate models. In this work, we follow the numerical method in Wu & Pan (2023) for the evaluation of the collision integral, with the necessary details described in the next subsection.

2.2. Numerical procedures

To simulate a physical problem representative of oceanic IGWs, we consider a horizontally isotropic domain with horizontal circular radius 42.4 km and vertical extent 2.1 km. This vertical extent is chosen to minimise the effects of surface and bottom boundaries, allowing a focus on IGW interactions in the ocean interior. The wavenumber domain is discretised using a 128×128 log-scale grid in both k and m, with wavenumber ranges $k \in [1.5 \times 10^{-4}, 1.6 \times 10^{-1}]$ m⁻¹ and $m \in [3.0 \times 10^{-3}, 3.2]$ m⁻¹. (Results using the log-scale grid and the previous linear grid (Wu & Pan 2023) do not show a statistically significant difference upon testing.) This set-up provides a spatial resolution as fine as 40 m horizontally and 2 m vertically.

The GM-like spectrum (Appendix A) is used as input to the WKE (2.1), specifically in terms \mathcal{F}_{p12} and \mathcal{F}_{1p2} . At an instantaneous time t, integrating the collision integral in (2.1) yields $\partial n(\mathbf{p})/\partial t$ and consequently $\partial E(\mathbf{p})/\partial t$. Invoking the conservation of spectral energy

$$\frac{\partial E(m)}{\partial t} + \frac{\partial \mathcal{P}(m)}{\partial m} = 0, \tag{2.3}$$

where $\partial E(m)/\partial t = \iint (\partial E(\mathbf{p})/\partial t) dk_x dk_y$, one can define the downscale energy flux $\mathcal{P}(m)$ across an arbitrary vertical wavenumber m

$$\mathcal{P}(m) = \int_0^m \frac{\partial E(m')}{\partial t} \, dm' = \int_0^m \left[\iint \frac{\partial E(k'_x, k'_y, m')}{\partial t} \, dk'_x \, dk'_y \right] dm'. \tag{2.4}$$

Instead of directly resolving turbulent events, the WKE evaluates the energy flux down to the 10 m vertical scale (represented by the critical vertical wavenumber $m_c = 0.62$ m⁻¹) as an estimate of the energy available for turbulent dissipation (Polzin *et al.* 2014). However, interpreting the WKE results near m_c is often constrained by potential violation of the weakly nonlinear assumption (Holloway 1978, 1980). Although recent studies have shown that $\mathcal{P}(m)$ exhibits low sensitivity to m near m_c (Wu & Pan 2023; Dematteis et al. 2024), we choose to further quantify this uncertainty by introducing a spectrumspecific cutoff vertical wavenumber m_{cutoff} (usually less than m_c), up to which no more than 10 % of waves violate the weakly nonlinear assumption, characterised by |Bo| > 0.2. It is important to acknowledge the gap between m_{cutoff} , beyond which the WKE becomes invalid, and m_c , at which IGWs become unstable to shear instability. Turbulent dissipation is approximated as the mean value of the downscale energy flux $\mathcal{P}(m)$ over the range $m \in [m_{cutoff}, m_c]$, when $m_{cutoff} < m_c$. The difference between the maximum and minimum values in $\mathcal{P}(m)$ over this range is introduced as the uncertainty. When $m_{cutoff} > m_c$, the WKE can be interpreted up to the dissipation scale without the breakdown of the weakly nonlinear assumption, thus the uncertainty associated with nonlinearity level becomes zero (although the choice of m_c may also exhibit uncertainty).

To evaluate the relative contribution of ID to the total turbulent dissipation, we isolate ID triads by applying a selection criterion based on the geometry of individual triads. We rank the frequencies of each wave component in a triad from high to low as $(\omega^H, \omega^M, \omega^L)$ and the magnitudes of vertical wavenumbers as $(|m^H|, |m^M|, |m^L|)$. As a scale-separated mechanism in both ω and m, an ID triad consists of a low- ω , low-m wave, and two high- ω , high-m waves (figure 1), satisfying $\omega^M/\omega^L > 4$ and $|m^M|/|m^L| > 4$. The threshold value for 'scale separation' is defined by a factor 4, as in Dematteis *et al.* (2024). Similar selection procedures have been adopted by Eden *et al.* (2019b) and Wu & Pan (2023).

3. Results

We start with the GM spectrum (Cairns & Williams 1976), then extend to spectra that deviate from GM, with a focus on the role of ID in turbulent dissipation across varying spectra. The direction of action diffusion, as described by (1.1), depends on the sign of σ , which is the vertical-wavenumber spectral slope of the action spectrum, $n \propto m^{\sigma}$. For GM-like spectra, $\sigma \equiv s_m - s_{\omega}$ represents the difference between the vertical-wavenumber and frequency spectral slopes of the energy spectrum in the high-frequency, high-vertical-wavenumber limit (see Appendix A for a detailed illustration). We consider the range $\sigma \in [-0.5, 0.5]$, corresponding to $s_m \in [-2.5, -1.5]$ with fixed $s_{\omega} = -2$, which is consistent with the range from global statistics of field measurements (Dematteis *et al.* 2024). The

energy level $E_0 = 3 \times 10^{-3} \text{ m}^{-2} \text{ s}^{-2}$, as defined in (A1), is kept constant as σ varies to ensure that the total energy of the IGW field remains unchanged. For comparison with GM, we present two extreme cases: a red spectrum with $\sigma = -0.5$, and a blue spectrum with $\sigma = 0.5$. We then explore the entire range $\sigma \in [-0.5, 0.5]$, followed by a sensitivity study with respect to the parameters E_0 and s_ω in Appendix B.

In the absence of generation and dissipation of IGWs, energy is conserved within a finite domain and redistributes through wave—wave interaction, with energy fluxes across the (spectral) domain boundaries remaining zero. Therefore, the rate of change of spectral energy density $\partial E/\partial t$ interprets spectral energy transfer within the domain, as shown in (2.3). Henceforth, we define regimes where $\partial E/\partial t < 0$ as sources, since their energy decays over time, supplying energy to other regimes. Conversely, regimes where $\partial E/\partial t > 0$ are sinks, since their energy increases, accumulating energy. The terms 'source' and 'sink' follow the conventions of Eden *et al.* (2019*a,b*), where they describe the direction of energy transfer rather than referring to specific generation or dissipation mechanisms.

3.1. The standard GM spectrum

For the GM spectrum characterised by a white action spectrum $n \propto m^0$ in the high-vertical-wavenumber limit, spectral energy transfer arising from all triad interactions exhibits a source between 2f and 4f, with sinks at lower and higher frequencies (figure 2a). The normalised Boltzmann rate (2.2) indicates that the high-m regime is subject to strong nonlinearity, casting doubt on the validity of the WKE results in this regime (figure 2c). The corresponding cutoff vertical wavenumber is $m_{cutoff} = 0.30 \text{ m}^{-1}$, a factor of 2 smaller than the critical vertical wavenumber $m_c = 0.62 \text{ m}^{-1}$. The total turbulent dissipation estimated by the WKE is $\mathcal{P} = (8.12 \pm 0.26) \times 10^{-10} \text{ W kg}^{-1}$ (figure 2d), in good agreement with the finescale parameterization prediction $\mathcal{P}_{FP} = 8 \times 10^{-10} \text{ W kg}^{-1}$, with the latter computed following the standard procedure described in Polzin et al. (2014). (These results correspond to a Coriolis frequency $f = 7.84 \times 10^{-5} \text{ s}^{-1}$ and a buoyancy frequency $N = 5.24 \times 10^{-3} \text{ s}^{-1}$ (Appendix A), which differ from the values used in Wu & Pan 2023.) Due to the vanishing gradient of the action spectrum in m, ID contributes almost no flux, except for some weak secondary diffusion (figures 2b,d), corroborating the findings of Dematteis et al. (2022).

3.2. A red action spectrum

For a typical red action spectrum characterised by $n \propto m^{-0.5}$ in the high-vertical-wavenumber limit, action and energy are more concentrated at large vertical scales compared to GM. With total energy held constant, action and energy at small scales are correspondingly reduced. Spectral energy transfer is dominated by a source between 2f and approximately 10f, with a sink below 2f and a much weaker sink above 20f (figure 3a). The magnitudes of the source and sinks, along with the downscale energy flux, are an order of magnitude smaller than those in GM (figures 3a,d). The weakly nonlinear assumption is better satisfied compared to that for GM, as indicated by the normalised Boltzmann rate (2.2) (figure 3c). The corresponding cutoff vertical wavenumber is $m_{cutoff} = 0.69 \text{ m}^{-1}$, allowing the WKE results to extend to the dissipation scale represented by $m_c = 0.62 \text{ m}^{-1}$ without introducing uncertainty associated with nonlinearity level as described in § 2.2.

ID exhibits a source above approximately 7f and two distinct sinks below 7f (figure 3b). The two sinks occur in separate regimes relative to the source: the first sink spreads over intermediate frequencies ($\omega \approx 5f$) and large vertical wavenumbers ($m \gtrsim 0.1 \text{ m}^{-1}$), while the second sink is concentrated near the inertial frequency ($\omega \approx f$)

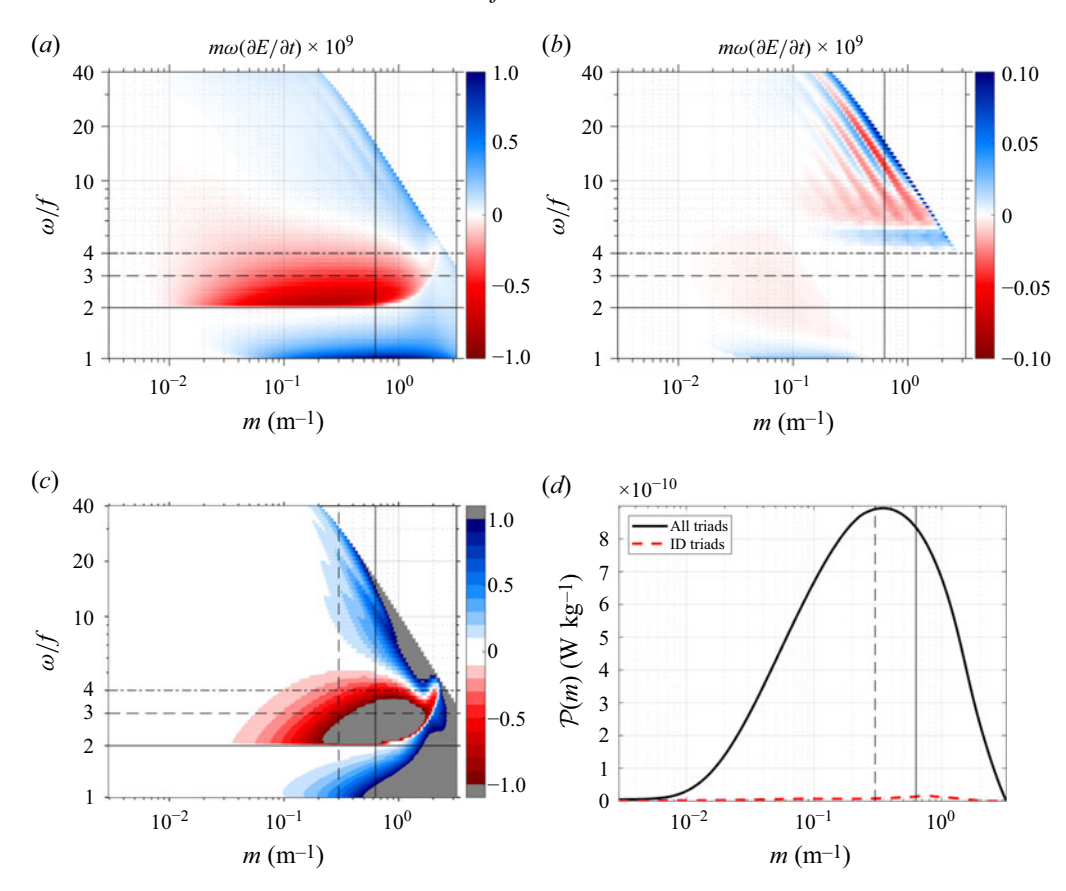


Figure 2. (a) Spectral energy transfer $m\omega$ ($\partial E/\partial t$) computed from the WKE (2.1) for the GM spectrum of the form $n \propto m^0$ in the high-m, high- ω limit. The prefactor $m\omega$ is included to preserve variance in the log-log representation. Energy sources ($\partial E/\partial t < 0$) and sinks ($\partial E/\partial t > 0$) are indicated in red and blue, respectively. (b) The same as (a), but retaining only the ID mechanism. (c) Normalised Boltzmann rate (2.2), where $|Bo| \ll 1$ indicates weak nonlinearity and the validity of the WKE. (d) Downscale energy flux (2.4), shown for all triads and for ID triads only. Horizontal lines in (a-c) denote frequencies 2f, 3f and 4f. Vertical solid and dashed lines denote the critical vertical wavenumber m_c and the cutoff vertical wavenumber m_{cutoff} , respectively.

and small vertical wavenumbers ($m \lesssim 0.1 \text{ m}^{-1}$). These three regimes – comprising the source and the two sinks – reflect the diffusive and scale-separated transfers characteristic of ID. In particular, the source and the first sink arise from the action diffusion at small scales described by (1.1), featuring a forward cascade in m accompanied by a backward cascade in ω . Since this diffusive transfer conserves action, it results in an energy surplus when moving towards lower frequencies, as energy is given by $E = n\omega$, and ω decreases. (This is more straightforward if we focus on a single triad (e.g. the one in figure 1). In this case, a red action spectrum leads to a forward diffusive transfer from p to p_2 . While action is conserved, i.e. $\Delta n = -\Delta n_2$, energy is not: the energy lost by p is always greater than that received by p_2 , i.e. $\omega \Delta n > \omega_2(-\Delta n_2)$, since $\omega > \omega_2$. This results in an energy surplus between p and p_2 , where excess energy must be absorbed by the large-scale mode p_1 , indicative of a backward scale-separated transfer.) To conserve total energy, excess energy must be absorbed by the large scale, leading to the formation of the second sink and enabling a scale-separated transfer that is backward in both m and ω .

Inclusion of both diffusive and scale-separated transfers is crucial to understanding the full picture of ID, as further illustrated by the ID-driven downscale energy flux $\mathcal{P}^{ID}(m)$

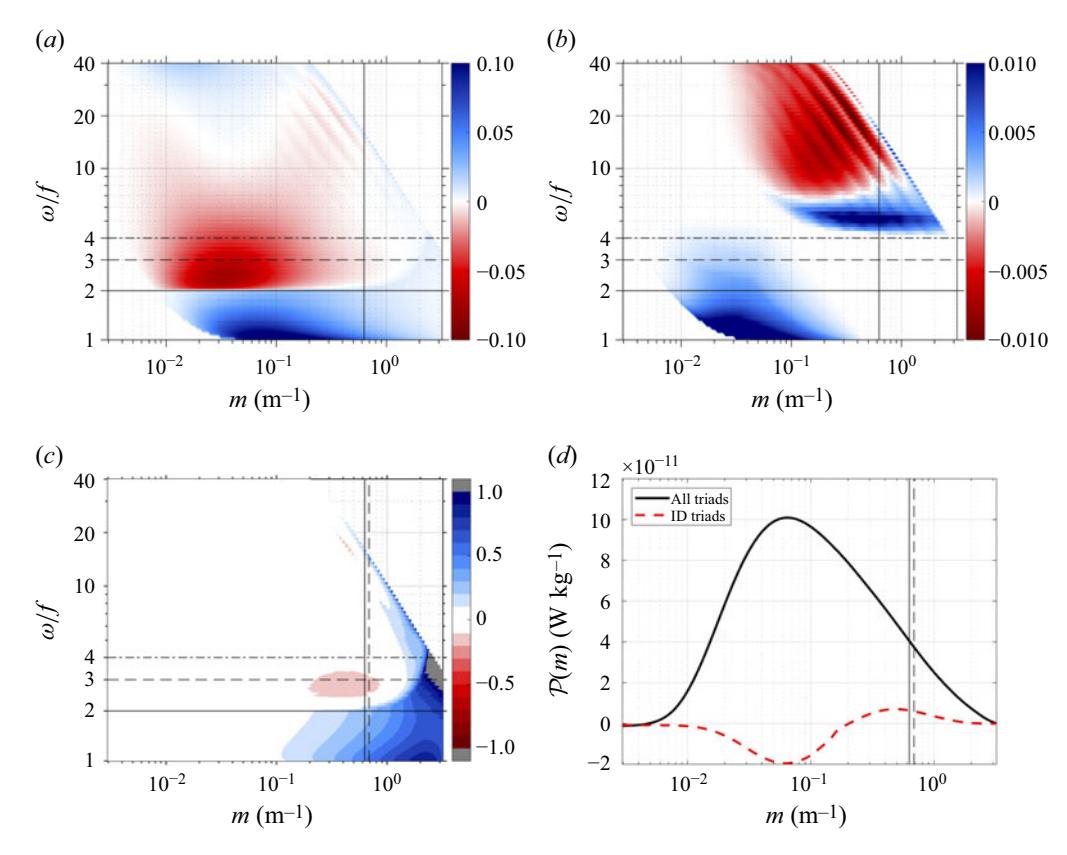


Figure 3. The same as figure 2 but for a red action spectrum, $n \propto m^{-0.5}$ in the high-m, high- ω limit. (a) $m\omega(\partial E/\partial t) \times 10^9$, (b) $m\omega(\partial E/\partial t) \times 10^9$, (c) Normalised Boltzmann rate, (d) Downscale energy flux.

(figure 3d). ID represents a backward cascade with $\mathcal{P}^{ID}(m) < 0$ when $m < 0.2 \text{ m}^{-1}$, and a forward cascade with $\mathcal{P}^{ID}(m) > 0$ when $m > 0.2 \text{ m}^{-1}$. The former results from the scale-separated transfer with the large scale as a sink, and the latter is governed by the diffusive transfer described by (1.1). At the dissipation scale, the ID-driven downscale energy flux is dominated by the diffusive transfer with $\mathcal{P}^{ID}(m_c) = (0.07 \pm 0.00) \times 10^{-10} \text{ W kg}^{-1}$, which contributes approximately 16% of the total turbulent dissipation $\mathcal{P}^{all}(m_c) = (0.41 \pm 0.00) \times 10^{-10} \text{ W kg}^{-1}$.

3.3. A blue action spectrum

For a typical blue action spectrum characterised by $n \propto m^{0.5}$ in the high-vertical-wavenumber limit, more action and energy are distributed to small vertical scales compared to GM. Spectral energy transfer is dominated by a source below 4f, with sinks below 1.5f and above 3f at $m \gtrsim 1~{\rm m}^{-1}$ (figure 4a). The magnitudes of the source and sinks, along with the downscale energy flux, are an order of magnitude greater than those in GM (figures 4a,d). Violation of the weakly nonlinear assumption is more pronounced, as indicated by the normalised Boltzmann rate (2.2) (figure 4c). The corresponding cutoff vertical wavenumber $m_{cutoff} = 0.12~{\rm m}^{-1}$ is significantly smaller than the critical vertical wavenumber $m_c = 0.62~{\rm m}^{-1}$, resulting in increased uncertainty associated with interpreting the WKE results in the strongly nonlinear regime (figure 4d).

ID manifests the reversed scenario relative to the red spectrum case presented in § 3.2. In particular, the diffusive transfer at small scales is now backwards towards lower m, 1021 A48-8

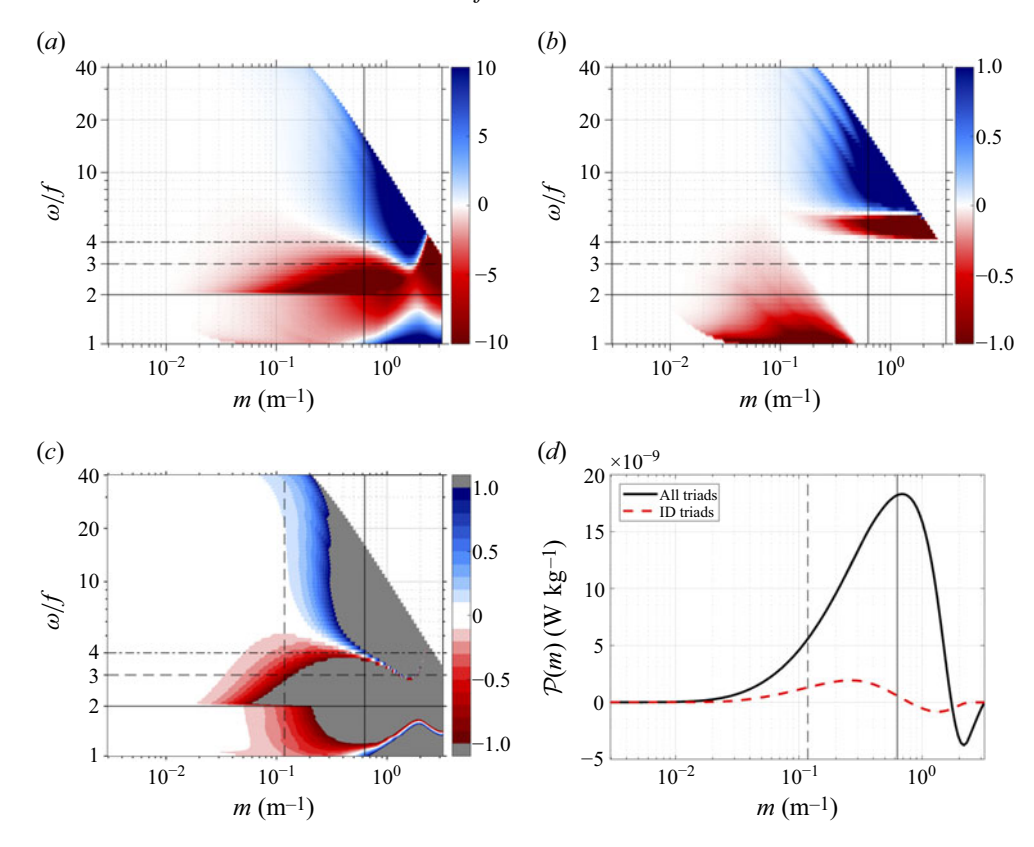


Figure 4. The same as figure 2 but for a blue action spectrum, $n \propto m^{0.5}$ in the high-m, high- ω limit. (a) $m\omega(\partial E/\partial t) \times 10^9$, (b) $m\omega(\partial E/\partial t) \times 10^9$, (c) Normalised Boltzmann rate, (d) Downscale energy flux.

and the scale-separated transfer is forwards, with energy sourced from the large scale to compensate for the deficit at small scales; see figure 4(b). (In this case, a blue action spectrum leads to a backward diffusive transfer from mode p_2 to mode p in a single triad (figure 1). The energy required by p is always greater than that supplied by p_2 , i.e. $\omega \Delta n > \omega_2(-\Delta n_2)$, given that $\omega > \omega_2$ and $\Delta n = -\Delta n_2$. This results in an energy deficit between p and p_2 , which will be compensated for by the large-scale mode p_1 , indicative of a forward scale-separated transfer.) However, the regime where the backward cascade dominates is confined to vertical scales smaller than the dissipation scale ($m > 0.8 \text{ m}^{-1}$), while the forward cascade regime spans a much broader range of m, encompassing both m_{cutoff} and m_c .

The downscale energy flux driven by ID is quantified as $\mathcal{P}^{ID} = (13 \pm 6.5) \times 10^{-10}$ W kg⁻¹ over the range between m_{cutoff} and m_c , accounting for 11 % of the total turbulent dissipation $\mathcal{P}^{all} = (120 \pm 63) \times 10^{-10}$ W kg⁻¹ (figure 4d). Within this range, the forward scale-separated transfer dominates the ID cascade, with energy fluxed downscale to sustain turbulent dissipation. As a result, despite its reversed direction relative to the red spectrum case, ID continues to act as a dissipative mechanism.

4. Discussion and conclusion

We begin by elaborating on and summarising the role of ID in ocean mixing for spectra deviating from the GM spectrum. At any given vertical wavenumber, the energy flux

Y.C. Wu and Y. Pan

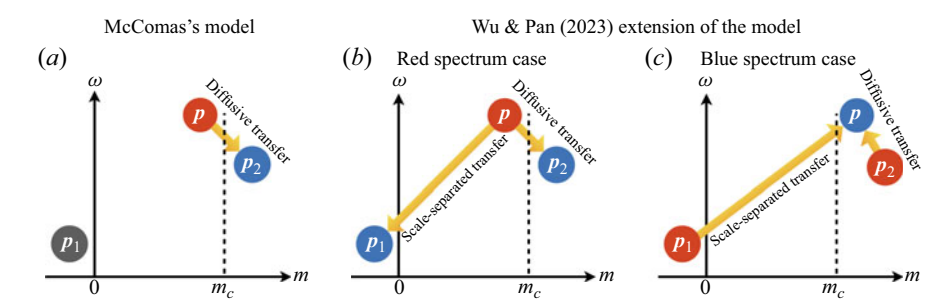


Figure 5. Conceptual models of ID for a resonant wave triad $p = p_1 + p_2$. The large-scale, near-inertial wave p_1 has an oppositely signed vertical wavenumber and thus appears to the left of the m = 0 axis (figure 1). (a) McComas' model illustrating a diffusive transfer from p to p_2 at small scales, while the large-scale wave p_1 remains stationary. (b,c) Our extension of the model for red ($\sigma < 0$) and blue ($\sigma > 0$) action spectra, $n \propto m^{\sigma}$, respectively. In both cases, a diffusive transfer (between p and p_2) and a scale-separated transfer (involving p_1) are highlighted, presenting ID as a broadband process rather than one confined to small scales. Red, blue and grey dots denote energy sources, sinks and stationary states, respectively. Yellow arrows indicate the direction of energy transfer. Turbulent dissipation is approximated by the downscale energy flux across the critical vertical wavenumber m_c .

comprises two components: a diffusive transfer described by (1.1), and a scale-separated transfer associated with energy absorption or compensation by the large scale. To facilitate energy fluxes across the dissipation scale represented by m_c and contribute to mixing, the diffusive transfer must involve triads with two high modes on each side of m_c , and the scale-separated transfer must involve triads with a low mode below m_c and two high modes above m_c . A complete picture of ID in the spatiotemporal domain is illustrated in figure 5. For red spectra with $\sigma < 0$ in $n \propto m^{\sigma}$, the diffusive transfer dominates near m_c , driving a forward cascade towards dissipation. As σ increases and passes zero (which corresponds to blue spectra with $\sigma > 0$), the scale-separated transfer becomes more and more important near m_c , where the energy compensation process supplies energy available for dissipation. While McComas's original conceptualisation of ID was based on a stationary large-scale field (figure 5a), our evaluation of the WKE reveals far richer dynamics of ID, in which the large scale actively participates in the energy cascade, and plays a crucial role in driving turbulent dissipation (figures 5b,c).

For a comprehensive evaluation of the role of ID across varying spectra, we swept the entire range $\sigma \in [-0.5, 0.5]$ using step size 0.1. The total turbulent dissipation increases dramatically with increasing σ , as bluer spectra allocate more energy to small scales and thus drive stronger turbulent dissipation (figure 6a). The WKE results align well with the finescale parameterization predictions for spectra that are close to GM. However, discrepancies increase as the spectra deviate from GM (figure 6a). This may be because finescale parameterization was primarily developed based on GM, which could lead to biased shear content estimates when applied to spectra that differ significantly from GM (Polzin et al. 2014). The relative contribution of ID is quantified as the turbulent dissipation driven by ID triads normalised by the total turbulent dissipation by all triads. For $\sigma = 0$, i.e. the GM spectrum, $\mathcal{P}^{ID}/\mathcal{P}^{all}$ is minimal due to the vanishing of both diffusive and scale-separated transfers; in this case, ID contributes almost no flux, despite some weak secondary diffusion (Dematteis et al. 2022; Wu & Pan 2023); see figure 6(b). Apart from this state, the relative contribution of ID remains consistently positive, and the ratio $\mathcal{P}^{ID}/\mathcal{P}^{all}$ is positively correlated with the deviation $|\sigma|$. At the two endpoints, $\sigma = \pm 0.5$, ID contributes up to 16% of the total dissipation. Moreover, the estimated uncertainty

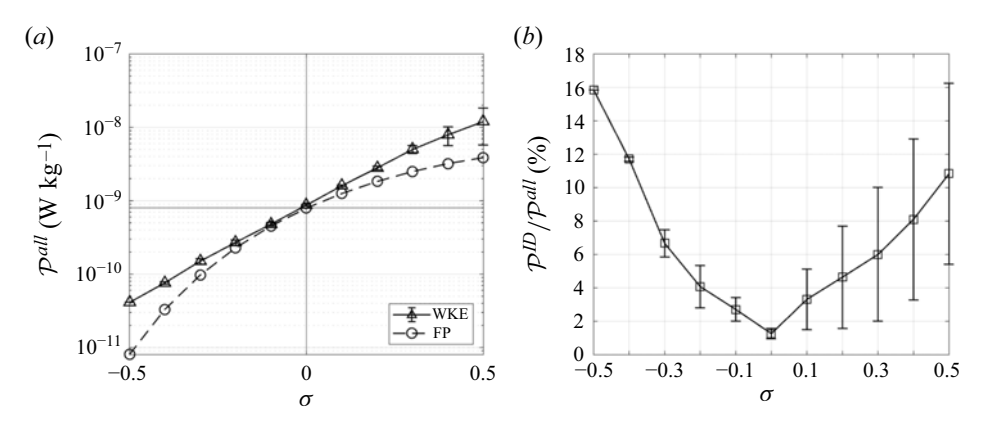


Figure 6. (a) Total turbulent dissipation \mathcal{P}^{all} estimated using the WKE compared with that obtained from finescale parameterization (FP). (b) Relative contribution of ID, $\mathcal{P}^{ID}/\mathcal{P}^{all}$, as a function of $\sigma \equiv s_m - s_\omega$. All results are based on fixed energy level $E_0 = 3 \times 10^{-3} \text{ m}^{-2} \text{ s}^{-2}$ and a constant frequency spectral slope $s_\omega = -2.0$. The error bars represent the uncertainty associated with nonlinearity level in $\mathcal{P}^{all}(m)$ and $\mathcal{P}^{ID}(m)/\mathcal{P}^{all}(m)$ over the range $m \in [m_{cutoff}, m_c]$, if $m_{cutoff} < m_c$. When $m_{cutoff} > m_c$, the uncertainty is zero.

associated with nonlinearity level grows with increasing σ , reflecting the widening gap between m_{cutoff} and m_c .

This study represents a significant step forward in understanding the role of ID in oceanic mixing. Unlike the empirical approach of finescale parameterization, the WKE captures the underlying mechanisms of wave—wave interactions, enabling diagnostic insights such as the role of ID, which constitutes the central focus of this study. Leveraging the WKE, we address long-standing theoretical gaps and provide a physically grounded depiction of ID in the spatiotemporal domain, without being restricted to the high- ω , high-m regime of the spectra, or relying on the diffusion (1.1) as a reduced-order alternative. By elucidating the dynamics of energy cascade in the IGW field, our findings offer valuable insights into the specific types of wave—wave interactions responsible for turbulent dissipation.

We conclude by placing two caveats on the present work. First, the analysis is based on the instantaneous energy transfer of GM-like spectra. The underlying assumption is that these spectra remain stationary under balanced forcing and dissipation in the ocean. An important direction is to examine the evolution of the spectra under wave—wave interactions within the WKE framework (see the recent work by Labarre, Krstulovic & Nazarenko 2025). Second, the present study assumes that the spectra retain a power-law form at small scales, even beyond the dissipation scale m_c . In practice, this assumption may be violated due to dissipative effects, which could result in a damped spectrum tail beyond m_c , and thus affect the interpretation of ID, especially in the case of blue spectra. A detailed investigation of this problem likely requires simulations of stratified turbulence. We leave this opportunity to future research.

Funding. This research is supported by the National Science Foundation (award OCE-2241495, OCE-2446007, OCE-2306124) and the Simons Foundation through Simons Collaboration on Wave Turbulence.

Declaration of interests. The authors report no conflict of interest.

Data availability statement. The data that support the findings of this study are openly available on GitHub at https://github.com/yue-cynthia-wu.

Appendix A. The GM spectrum and variations

The spectral representation of oceanic IGWs was first modelled by Peter H. Garrett and Walter H. Munk in the 1970s in a series of publications (Garrett & Munk 1972, 1975; Cairns & Williams 1976), providing a statistical and empirical description of the wave energy distribution based on the frequency and vertical wavenumber of IGWs

$$E(\omega, m) = \frac{N}{N_0} E_0 A(m) B(\omega), \tag{A1}$$

where $E(\omega, m)$ is the wave energy in the frequency-vertical wavenumber domain. The factor N/N_0 is a stratification scaling, where N and $N_0 = 5.24 \times 10^{-3} \text{ s}^{-1}$ are the actual and reference buoyancy frequencies, respectively. The parameter E_0 is the energy level of the IGW field.

Functions A and B in (A1) are separable with respect to m and ω , and are normalised to integrate to unity such that the total energy is $\iint E(\omega, m) d\omega dm = (N/N_0)E_0$

$$A(m) \propto \frac{1}{m^*} \left[1 + \left(\frac{m}{m^*} \right)^r \right]^{s_m/r}, \tag{A2}$$

$$B(\omega) \propto \omega^{s_{\omega} - 2s_{NI}} \left(\omega^2 - f^2\right)^{s_{NI}},$$
 (A3)

where $m^* = \pi j/b$ is the characteristic vertical wavenumber, j is the mode number, and b is the stratification scale height. The parameter r controls the steepness of the transition from the low-m plateau to the high-m power-law regime; r=2 is commonly used, as alternative values are rarely confirmed observationally. The Coriolis or inertial frequency $f=2\Omega\sin\varphi$ is a function of latitude φ , where $\Omega=7.29\times10^{-5}~{\rm s}^{-1}$ is the Earth's rotational angular velocity. The spectrum is characterised by three spectral slopes: s_{NI} in the near-inertial frequency limit, s_{ω} in the high- ω limit, and s_m in the high-vertical-wavenumber limit. Common to all variations of GM is the presence of an inertial peak and red spectra in both ω and m, signifying a concentration of energy near the inertial frequency and in low vertical modes (Polzin & Lvov 2011).

For the standard GM spectrum described in Cairns & Williams (1976), the parameters are j=4 and b=1300 m, so $m^*=0.01$ m $^{-1}$. The buoyancy frequency is $N=N_0=5.24\times 10^{-3}$ s $^{-1}$, and the Coriolis frequency is $f=7.84\times 10^{-5}$ s $^{-1}$, corresponding to the latitude $\varphi=32.5^\circ$ for mid-latitude oceans. The energy level is $E_0=3\times 10^{-3}$ m $^{-2}$ s $^{-2}$. The three spectral slopes are $s_\omega=s_m=-2$ and $s_{NI}=-0.5$.

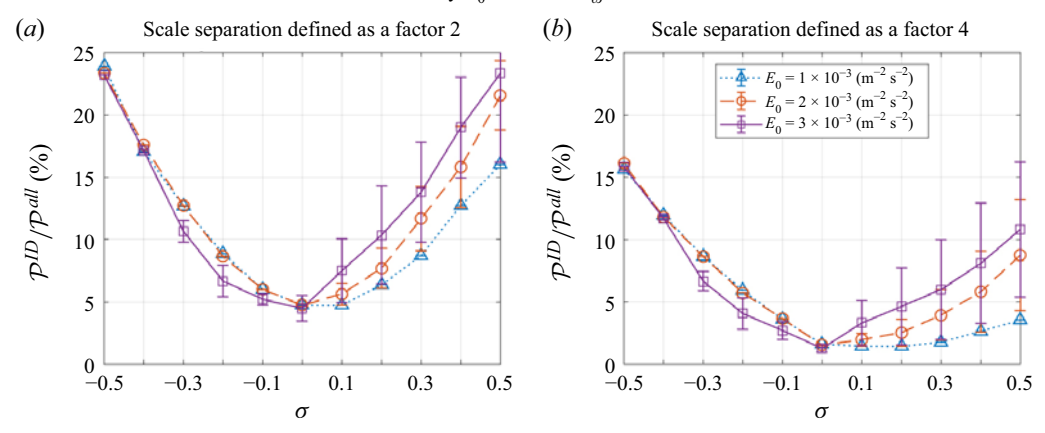
The energy spectrum given by (A1) follows power-law scaling in the high- ω , high-m regime, expressed as $E(\omega, m) \propto \omega^{s_{\omega}} m^{s_{m}}$. This corresponds to an action spectrum $n(k, m) \propto k^{s_{\omega}-2} m^{s_{m}-s_{\omega}}$. The conversion adheres to the relationship

$$n(k,m) = \frac{E(k,m)}{\omega} = \frac{E(\omega,m)}{2\pi k\omega} \frac{\partial \omega}{\partial k} = \frac{E(\omega,m)}{2\pi k\omega} \frac{N^2 - \omega^2}{k^2 + m^2}.$$
 (A4)

Appendix B. Sensitivity study to parameters E_0 and s_{ω}

The results presented in § 3 are based on fixed values for the energy level $E_0 = 3 \times 10^{-3}$ m⁻² s⁻² and the frequency spectral slope $s_{\omega} = -2.0$, with 'scale separation' defined at a factor 4. To validate our conclusions across a broader parameter space, a sensitivity study has been conducted (figure 7). When the frequency spectral slope is held fixed at $s_{\omega} = -2.0$ (figures 7a,b), the effect of E_0 on the relative contribution of ID to the total turbulent dissipation $\mathcal{P}^{ID}/\mathcal{P}^{all}$ vanishes for the two reddest spectra ($\sigma \leq -0.4$). In this regime, the weakly nonlinear assumption holds up to the dissipation scale ($m_{cutoff} > m_c$), so the downscale energy flux is evaluated solely across a constant m_c . As a result, E_0

Vary E_0 with fixed $s_{\infty} = -2.0$



Vary s_{ω} with fixed $E_0 = 3 \times 10^{-3} \text{ (m}^{-2} \text{ s}^{-2}\text{)}$

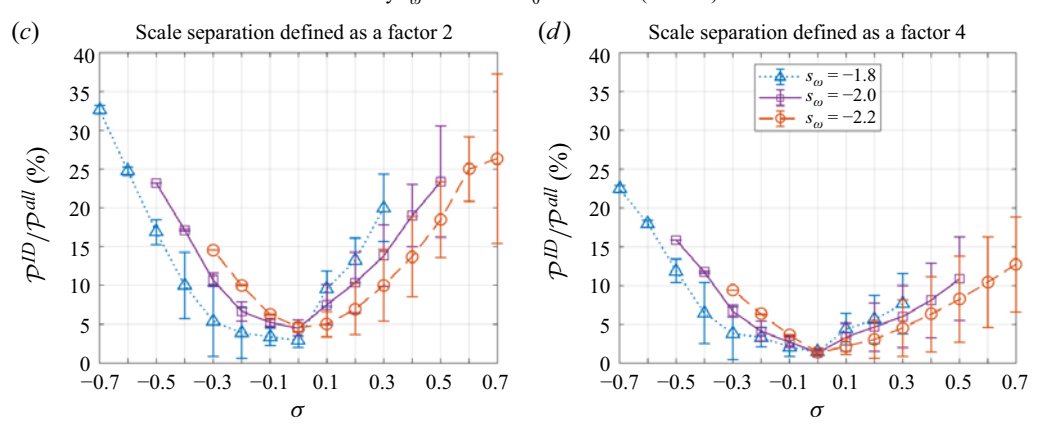


Figure 7. Relative contribution of ID to the total turbulent dissipation, $\mathcal{P}^{ID}/\mathcal{P}^{all}$, as a function of $\sigma \equiv s_m - s_\omega$, for cases with 'scale separation' defined at factor (a,c) 2 and (b,d) 4. (a,b) Results for varying energy levels E_0 with fixed frequency spectral slope $s_\omega = -2.0$. (c,d) Results for varying s_ω with fixed $E_0 = 3 \times 10^{-3}$ m⁻² s⁻².

factors out when evaluating $\mathcal{P}^{ID}/\mathcal{P}^{all}$. In contrast, the effect of E_0 becomes increasingly prominent for bluer spectra when $m_{cutoff} < m_c$. The greater the value of E_0 , the wider the separation between m_{cutoff} and m_c , introducing increased uncertainty in the prediction of turbulent dissipation using the WKE.

Despite the influences of E_0 and s_ω , the main conclusion of this study remains robust, even under a less stringent definition of 'scale separation' (i.e. a factor 2; see figures 7a,c). When both diffusive and scale-separated transfers are considered, ID always contributes positively to turbulent dissipation and acts as a dissipative mechanism.

REFERENCES

CAIRNS, J.L. & WILLIAMS, G.O. 1976 Internal wave observations from a midwater float, 2. *J. Geophys. Res.* 81 (12), 1943–1950.

DELPECH, A., BARKAN, R., SRINIVASAN, K., MCWILLIAMS, J.C., ARBIC, B.K., SIYANBOLA, O.Q. & BUIJSMAN, M.C. 2024 Eddy—internal wave interactions and their contribution to cross-scale energy fluxes: a case study in the California current. *J. Phys. Oceanogr.* **54** (3), 741–754.

Y.C. Wu and Y. Pan

- DEMATTEIS, G., BOYER, L., ARNAUD, P., FRIEDERIKE, P., KURT, L., ALFORD, M.H., WHALEN, C.B. & LVOV, Y.V. 2024 Interacting internal waves explain global patterns of interior ocean mixing. *Nat. Commun.* 15 (1), 7468.
- DEMATTEIS, G. & LVOV, Y.V. 2021 Downscale energy fluxes in scale-invariant oceanic internal wave turbulence. *J. Fluid Mech.* **915**, A129.
- DEMATTEIS, G., POLZIN, K. & LVOV, Y.V. 2022 On the origins of the oceanic ultraviolet catastrophe. J. Phys. Oceanogr. 52 (4), 597–616.
- DONG, W., BÜHLER, O. & SMITH, K.S. 2020 Frequency diffusion of waves by unsteady flows. *J. Fluid Mech.* **905**, R3.
- Dong, W., Bühler, O. & Smith, K.S. 2023 Geostrophic eddies spread near-inertial wave energy to high frequencies. *J. Phys. Oceanogr.* **53** (5), 1311–1322.
- EDEN, C., CHOUKSEY, M. & OLBERS, D. 2019a Gravity wave emission by shear instability. J. Phys. Oceanogr. 49 (9), 2393–2406.
- EDEN, C., POLLMANN, F. & OLBERS, D. 2019b Numerical evaluation of energy transfers in internal gravity wave spectra of the ocean. J. Phys. Oceanogr. 49 (3), 737–749.
- EDEN, C., POLLMANN, F. & OLBERS, D. 2020 Towards a global spectral energy budget for internal gravity waves in the ocean. *J. Phys. Oceanogr.* **50** (4), 935–944.
- GARRETT, C. & MUNK, W. 1972 Space-time scales of internal waves. Geophys. Fluid Dyn. 3 (3), 225-264.
- GARRETT, C. & MUNK, W. 1975 Space–time scales of internal waves: a progress report. *J. Geophys. Res.* **80** (3), 291–297.
- GREGG, M.C. 1989 Scaling turbulent dissipation in the thermocline. J. Geophys. Res. Oceans 94 (C7), 9686–9698.
- HASSELMANN, K. 1966 Feynman diagrams and interaction rules of wave-wave scattering processes. *Rev. Geophys.* 4 (1), 1–32,
- HASSELMANN, K., SAFFMAN, P.G. & LIGHTHILL, M.J. 1967 Nonlinear interactions treated by the methods of theoretical physics (with application to the generation of waves by wind). *Proc. R. Soc. Lond. A: Math. Phys. Sci.* 299 (1456), 77–103.
- HENYEY, F.S., WRIGHT, J. & FLATTÉ, S.M. 1986 Energy and action flow through the internal wave field: an eikonal approach. *J. Geophys. Res. Oceans* **91** (C7), 8487–8495,
- HOLLOWAY, G. 1978 On the spectral evolution of strongly interacting waves. *Geophys. Astrophys. Fluid Dyn.* 11 (1), 271–287.
- HOLLOWAY, G. 1980 Oceanic internal waves are not weak waves, J. Phys. Oceanogr. 10 (6), 906–914.
- KAFIABAD, H.A., SAVVA, M.A.C. & VANNESTE, J. 2019 Diffusion of inertia-gravity waves by geostrophic turbulence. *J. Fluid Mech.* **869**, R7.
- KUNZE, E., SMITH, L. & STEFAN, G. 2004 The role of small-scale topography in turbulent mixing of the global ocean. *Oceanography* 17 (1), 55–64.
- LABARRE, V., AUGIER, P., KRSTULOVIC, G. & NAZARENKO, S. 2024a Internal gravity waves in stratified flows with and without vortical modes. *Phys. Rev. Fluids* 9, 024604.
- LABARRE, V., KRSTULOVIC, G. & NAZARENKO, S. 2025 Wave-kinetic dynamics of forced-dissipated turbulent internal gravity waves. *Phys. Rev. Lett.* **135**, 014101.
- LABARRE, V., LANCHON, N., CORTET, P.-P., KRSTULOVIC, G. & NAZARENKO, S. 2024b On the kinetics of internal gravity waves beyond the hydrostatic regime. *J. Fluid Mech.* **998**, A17.
- LANCHON, N. & CORTET, P.P. 2023 Energy spectra of nonlocal internal gravity wave turbulence. *Phys. Rev. Lett.* **131**, 264001.
- LVOV, Y. & TABAK, E.G. 2004 A Hamiltonian formulation for long internal waves. *Phys. D Nonlinear Phenom.* **195** (1), 106–122.
- Lvov, Y.V., Polzin, K.L., Tabak, E.G. & Yokoyama, N. 2010 Oceanic internal-wave field: theory of scale-invariant spectra. *J. Phys. Oceanogr.* 40 (12), 2605–2623.
- LVOV, Y.V., POLZIN, K.L. & YOKOYAMA, N. 2012 Resonant and near-resonant internal wave interactions. J. Phys. Oceanogr. 42 (5), 669–691.
- Lvov, Y.V. & TABAK, E.G. 2001 Hamiltonian formalism and the Garrett–Munk spectrum of internal waves in the ocean. *Phys. Rev. Lett.* **87**, 168–501.
- McComas, C.H. 1977 Equilibrium mechanisms within the oceanic internal wave field. *J. Phys. Oceanogr.* 7 (6), 836–845.
- McComas, C.H. & Bretherton, F.P. 1977a Resonant interaction of oceanic internal waves. *J. Geophys. Res.* 82 (9), 1397–1412,
- MCCOMAS, C.H. & BRETHERTON, F.P. 1977b Resonant interaction of oceanic internal waves. J. Geophys. Res. 82 (9, Mar.20, 1977), 1397–1412.

- McComas, C.H. & Müller, P. 1981a The dynamic balance of internal waves. J. Phys. Oceanogr. 11 (7), 970–986.
- MCCOMAS, C.H. & MÜLLER, P. 1981b Time scales of resonant interactions among oceanic internal waves. J. Phys. Oceanogr. 11 (2), 139–147.
- MÜLLER, P. & OLBERS, D.J. 1975 On the dynamics of internal waves in the deep ocean. *J. Geophys. Res.* **80** (27), 3848–3860,
- NAZARENKO, S. 2011 Wave Turbulence. Springer.
- OLBERS, D.J. 1974 On the Energy Balance of Small-scale Internal Waves in the Deep-sea. G.M.L. Wittenborn.
 OLBERS, D.J. 1976 Nonlinear energy transfer and the energy balance of the internal wave field in the deep ocean. J. Fluid Mech. 74 (2), 375–399.
- PAN, Y., ARBIC, B.K., NELSON, A.D., MENEMENLIS, D., PELTIER, W.R., Xu, W. & Li, Y. 2020 Numerical investigation of mechanisms underlying oceanic internal gravity wave power-law spectra. *J. Phys. Oceanogr.* **50** (9), 2713–2733.
- POLZIN, K.L. & LVOV, Y.V. 2011 Toward regional characterizations of the oceanic internal wavefield. *Rev. Geophys.* **49** (4).
- POLZIN, K.L., NAVEIRA GARABATO, A.C., HUUSSEN, T.N., SLOYAN, B.M. & WATERMAN, S. 2014 Finescale parameterizations of turbulent dissipation. *J. Geophys. Res. Oceans* **119** (2), 1383–1419,
- POLZIN, K.L., TOOLE, J.M. & SCHMITT, R.W. 1995 Finescale parameterizations of turbulent dissipation. J. Phys. Oceanogr. 25 (3), 306–328.
- SAVVA, M.A.C., KAFIABAD, H.A. & VANNESTE, J. 2021 Inertia-gravity-wave scattering by three-dimensional geostrophic turbulence. *J. Fluid Mech.* 916, 1–30.
- SKITKA, J., ARBIC, B.K., THAKUR, R., MENEMENLIS, D., PELTIER, W.R., PAN, Y., MOMENI, K. & MA, Y. 2024 Probing the nonlinear interactions of supertidal internal waves using a high-resolution regional ocean model. *J. Phys. Oceanogr.* **54** (2), 399–425.
- WU, Y. & PAN, Y. 2023 Energy cascade in the Garrett–Munk spectrum of internal gravity waves. J. Fluid Mech. 975, A11.
- ZAKHAROV, V.E., LVOV, V.S. & FALKOVICH, G. 1992 Kolmogorov Spectra of Turbulence. Springer-Verlag.